Heliyon 9 (2023) e21678

Contents lists available at ScienceDirect

Heliyon

journal homepage: www.cell.com/heliyon

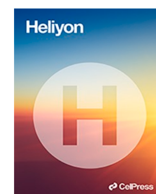

Bacterial MgSe complex nanoparticle synthesis and electrical characterization of fabricated Ag/MgSe/p-Si hetero-structure under dark and illumination

T. Çakıcı [a], Ö. Gür Özdal [b], N. Almousa [c], F. Yıldız [d], E. Kavaz Perişanoğlu [d], H. Khalil [e], Antoaneta Ene [f,**], Hesham M.H. Zakaly [g,h,*]

[a] Department of Electrical and Energy, Ispir Hamza Polat Vocational School of Higher Education, Ataturk University, Erzurum, Turkey
[b] Department of Biology, Science Faculty Ataturk University, Erzurum, Turkey
[c] Department of Physics, College of Science, Princess Nourah bint Abdulrahman University.P.O.Box 84428, Riyadh, 11671, Saudi Arabia
[d] Department of Physics, Science Faculty Ataturk University, Erzurum, Turkey
[e] City of Scientific Research and Technological Application (SRTA-City), Alexandria, 21934, Egypt
[f] INPOLDE Research Center, Department of Chemistry, Physics and Environment, Faculty of Sciences and Environment, Dunarea de Jos University of Galati, 47 Domneasca Street, 800008, Galati, Romania
[g] Istinye University, Faculty of Engineering and Natural Sciences, Computer Engineering Department, Istanbul, 34396, Turkey
[h] Institute of Physics and Technology, Ural Federal University, 620002, Yekaterinburg, Russia

ARTICLE INFO

Keywords:
Nanoparticles
Bacterial synthesis
MgSe
Thin film
I–V
C–V

ABSTRACT

The *Pseudomonas aeruginosa* OG1 strain was used in the bacterial synthesis of MgSe compound nanoparticles. The obtained samples were subsequently shaped into nanocrystalline MgSe films, and their optical, structural, morphological, and electrical properties were assessed on glass and p-Si substrates. Structural and morphological characterizations showed that the fabricated thin film samples have a polycrystalline structure with high quality and uniform grain sizes. The MgSe films produced on glass substrates exhibit a direct spectral band gap of 2.53 eV, according to optical measurements. The Ag/MgSe/p-Si layered diode structure was fabricated using the produced MgSe nanoparticles and then characterized by electrical properties. Electrical measurements were carried out under these two conditions to assess the effects of dark and illumination conditions on the band dynamics of the heterostructure devices. Under illumination, the barrier height decreased while the interface density states distribution increased. These measurements showed that using bacterial-assisted grown MgSe nanocrystalline films, the developed Ag/MgSe/p-Si device structure exhibited a remarkable photoresponse and stable rectifying property. Green synthesis methods for the production of these nanocrystalline materials have the potential to offer low-cost alternatives for photosensitive applications.

* Corresponding authors. Institute of Physics and Technology, Ural Federal University, 620002, Yekaterinburg, Russia.
** Corresponding authors. INPOLDE Research Center, Department of Chemistry, Physics and Environment, Faculty of Sciences and Environment, Dunarea de Jos University of Galati, Romania.
E-mail addresses: antoaneta.ene@ugal.ro (A. Ene), h.m.zakaly@gmail.com, hesham.zakaly@istinye.edu.tr (H.M.H. Zakaly).

https://doi.org/10.1016/j.heliyon.2023.e21678
Received 7 April 2023; Received in revised form 21 October 2023; Accepted 25 October 2023
Available online 26 October 2023
2405-8440/© 2023 Published by Elsevier Ltd. This is an open access article under the CC BY-NC-ND license (http://creativecommons.org/licenses/by-nc-nd/4.0/).

1. Introduction

Nanotechnology is the study and management of matter at the nanoscale, with dimensions ranging from 1 to 100 nm. The capacity to design, manipulate, and fabricate materials at the nanoscale is central to nanotechnology. These substances are known as nanomaterials.

Nanomaterial-based commercial procedures and items are quickly expanding, and these tiny materials are widely found in paints, textiles, cosmetics, electronics, agriculture, engineering, and medicine. With the advancement of nanotechnology and nanomaterials, the synthesis of distinct particles has grown in importance [1–5]. The sizes and quantum properties of nanoparticles give them new physicochemical properties [6]. Physical approaches are expensive because of the energy required to maintain the high vacuum and temperature used in NPs production. Chemical methods to synthesis nanoparticles include toxic and non-environmental-friendly processes [7].

With the rapid increase in the demand for nanomaterials, the production and use of nanomaterials obtained by traditional methods have also increased. At the same time, the negative impact of nanomaterials obtained by conventional methods on the environment will increase. As a result, there is a demand for green nanomaterials that are not only cost-effective but also safe for people and the environment. Moreover, thin film deposition operations may be carried out at low temperatures using non-toxic gases.

In recent years, green production of metallic nanoparticles has emerged as a new and promising subject of study. The rising demand for "green" and cost-effective metal nanoparticle manufacturing techniques has motivated researchers to investigate the use of microorganisms, plant extracts, and other biomaterials [8,9,13,14]. Microbial synthesis is a good alternative to traditional nanoparticle synthesis methods due to its superior features, such as being inexpensive, safe, simple and non-toxic. Microbial synthesis has allowed the production of biocompatible, stable, and safe nanoparticles. Because of its low cost and environmental friendliness, the synthesis of different nanoparticles using microbial agents such as algae, fungus, bacteria, enzymes, peptides, organic acids, and yeast has piqued the interest of many biomedical researchers [9–12]. Because of its low cost and environmental friendliness, the synthesis of different nanoparticles by microbial agents such as algae, fungus, bacteria, enzymes, peptides, organic acids, and yeast has piqued the interest of many medicinal researchers [15,16].

Due to their characteristics and practicality, heterostructured semiconductors consisting of II-VI compounds with wide-band gaps have received a lot of interest. These semiconductors are especially used in laser diodes [17] and many optoelectronic devices [18]. Researchers have focused on preparing nanostructured semiconductors in the last decade using economically inexpensive and simple methods [19,20]. Materials from the alkaline earth chalcogenide group, such as CuSe, CaSe, ZnSe, and MgSe, have gained interest due to their use in a variety of optoelectronic devices. However, mainly have luminescence properties; this group has attracted attention [21]. Scientific societies investigating semiconductor devices such as quantum cascade formations, quantum well-infrared photosensors, yellow laser diodes, and emitters are particularly interested in group II-VI selenite quantum well structures [22]. MgSe quantum well structures, in particular, built with the selenide group, have been established as a viable alternative to conventional semiconductor systems for optical communication applications with wavelengths of 1.55 mm [23,24]. MgSe is a critical component of semiconductors with a large band gap that may be manufactured in a variety of dimensions and NP structures.

In our research paper, the deposition and characterization of MgSe compound nanoparticles produced using the bacterial synthesis method as a MgSe thin film on p-type Si were previously reported as MgSe/p-Si heterojunction [25]. Current-voltage (I–V) and capacitance-voltage (C–V) measurements were done under dark and illumination conditions to investigate the electrical characteristics of the Ag/MgSe/p-Si/Al heterojunction diode produced in this work.

2. Experimental

This study was conducted in two parts. At the initial stage, MgSe nanoparticles were synthesized utilizing a green process, which, when compared to standard procedures, does not result in dangerous compounds in the products resulting from chemicals.

2.1. Bacterial synthesized MgSe NP solution and MgSe thin film fabrication on glass and p-Si substrates

MgSe compound nanoparticles obtained by *bacteria (Pseudomonas aeruginosa)* OG1 strain. This experimental step was reported in our previous research [25]. Then, the supernatant and insoluble cell fraction interface were removed [11], and a deionized water solution, including the cleaned and suspended MgSe nanoparticles, was obtained. After that, the mixture was divided into two beakers. One of these suspensions was used to synthesize a MgSe thin film on a glass substrate for UV-VIS measurements; the other was used to make an Ag/MgSe/p-Si/Al diode structure onto a p-Si substrate for XRD, AFM, FE-SEM, and EDS measurements, as well as I–V and C–V measurements, for characterization and electrical properties, respectively. The I–V measurements of the Ag/MgSe/p-Si/Al heterojunction diode structure have been investigated at room temperature, both in the dark and in the light.

2.2. Fabrication and characterization of the Ag/MgSe/p-Si/Al diode structure

This section reported the fabrication and techniques for electrically analyzing the Ag/MgSe/p-Si/Al diode structure. To obtain this diode, we first put the p-Si substrate in a vacuum environment at a pressure of 1×10^{-5} Tor. Then, using thermally evaporating Al, we formed an ohmic contact between Al and the back of the p-Si substrate. The p-Si/Al structure was then annealed at about 550 °C for 3 min in a flowing media of dry nitrogen to reduce the resistivity of the aluminium ohmic contact. The MgSe nanoparticles solution was then put onto the p-Si substrate and dried for 60 min at 65 °C on a heated copper plate. As a result, a thin layer of MgSe was applied to

the p-Si substrate. Finally, a cylindrical shadow mask with a 1.00 mm diameter size was applied to the MgSe thin film surface. Then it was put in a vacuum system (1.5 10^{-5} Torr), and Ag metallic contact was formed, directly evaporating the Ag. The Ag/MgSe/p-Si/Al device structure was consequently constructed.

The characterizations of the MgSe thin prepared films on glass and p-Si substrates were realized after their fabrication. Then, a UV–visible spectrometer (PerkinElmer Lambda 2S UV–Visible spectrometer) was used to evaluate the optical characteristics of the MgSe thin film sample that had been produced onto the glass substrate. The crystal structure of the MgSe thin film that was produced on the p-Si substrate, on the various other hands, was evaluated using an X-ray diffractometer (XRD Bruker D2 Kα, λ = 1.54 Å, scanning angle 70°). AFM (Hitachi 5100 N) and FE-SEM measurements were used to assess the surface morphological characteristics of the samples, and EDX connected with FE-SEM (Sigma 300 Model Zeiss Gemini) was employed to deduce the compound content of each sample. Besides that, I–V and C–V measurements were performed to assess the electrical characteristics of the Ag/MgSe/p-Si/Al diode structure. The measuring equipment employed was computer-controlled the. Picoammeter/Voltage Source Meter (Keitley 487 Picoammeter/Voltage Source) and Low-Frequency Impedance Analyzer (HP 4192A, 50–13 MHz LF Impedance Analyzer). Fig. 1 has shown Ag/MgSe/p-Si/Al device structure and energy band diagram at the thermal equilibrium.

3. Results and discussion

3.1. MgSe thin film optical, structural, and morphological analysis

This section and Fig. 2 (a), (b), (c), (d), (e), and (f) detailed discussed our previous research article [25]. For the readers in this study, we summarized here once more briefly the results that we reported on the MgSe thin film characteristics for the MgSe/p-Si structure in our previous research [25].

The optical band gap energy value of the MgSe thin film was determined to be 2.53 eV using the extrapolation method to the linear section of the curve, also illustrated in Fig. 2 (a), which shows the optical absorption spectrum of the MgSe thin film formed onto glass substrate function of wavelength in a range ranging from 300 to 1000 nm.

The XRD spectra of the MgSe thin film deposited onto the p-Si substrate are displayed in Fig. 2 (b). Two peaks could well be detected in Fig. 2 (b) along the directed planes at (111) and (200). The findings from (JCPDS card no. 18–0777) indicate that the cubic lattice of the MgSe thin film could be observed in this crystalline phase. Similar results from several research in the literature are well supported by the patterns that have been noticed [25–28]. The highest peak is p-Si, which displays cubic crystallization at the (100) directional plane. The average crystallite size, D, and the spacing between the planes, d, of the MgSe thin film formed on the p-Si substrate were

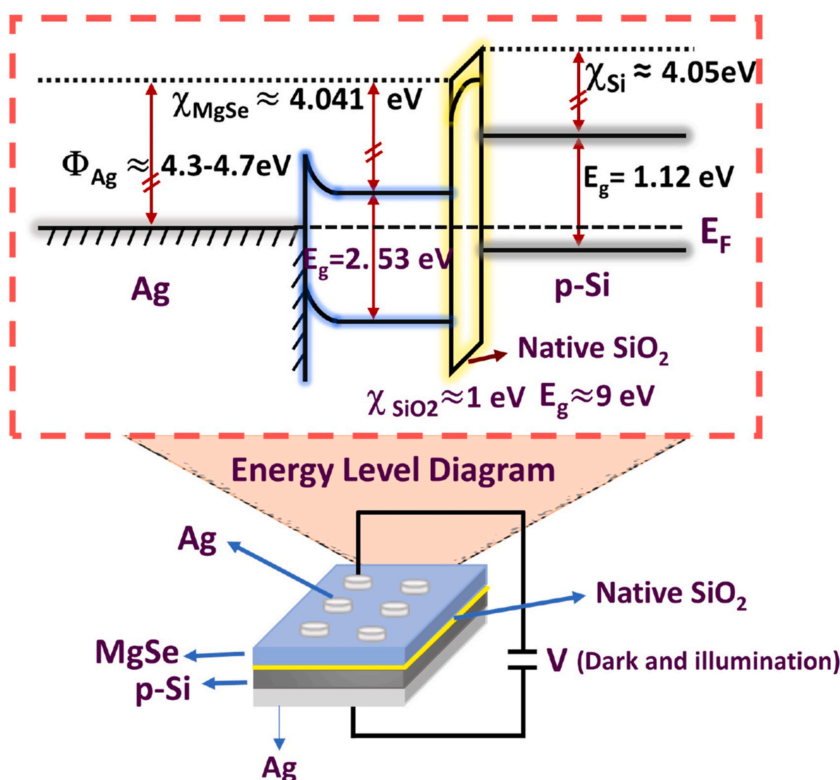

Fig. 1. Producing an Ag/MgSe/p-Si/Al device structure with the proposed energy level diagram in thermal equilibrium involves converting MgSe nanoparticles made via bacterial fabrication into a thin film interface.

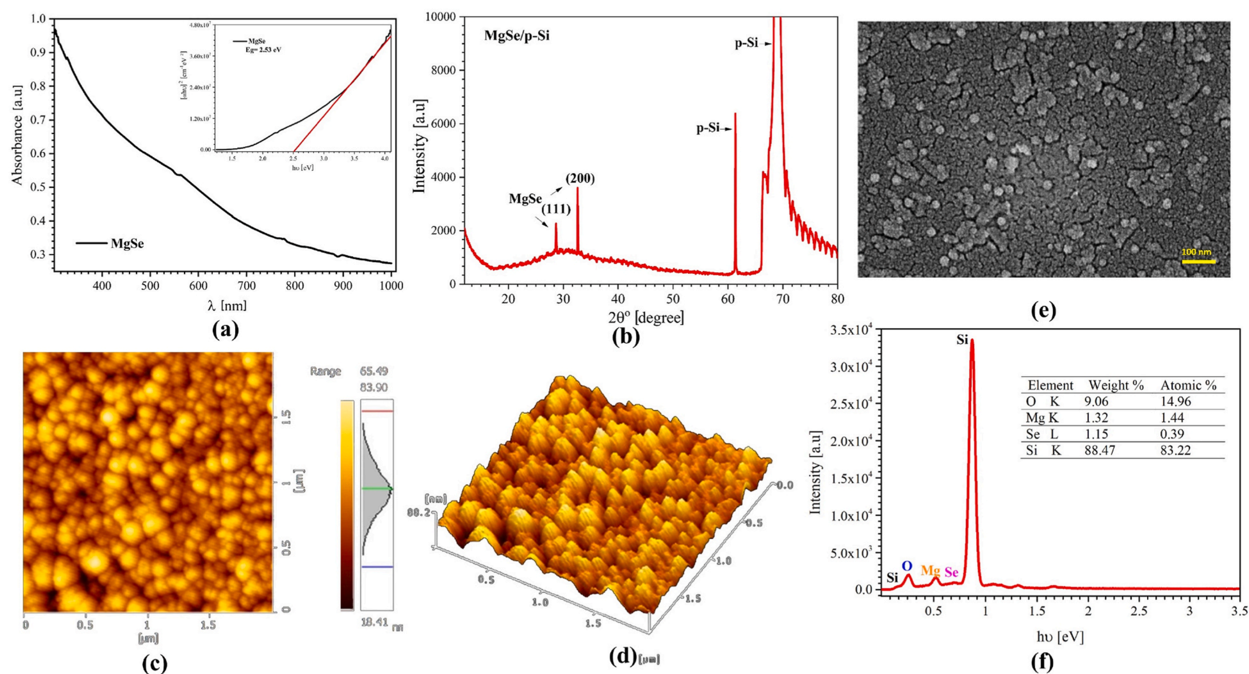

Fig. 2. (a) Plots of optical absorbance vs. wavelength (nm), and $(\alpha h\upsilon)^2$ vs. hυ, respectively, for a room-temperature MgSe film that is grown onto a glass substrate. **(b)** MgSe thin film deposited on p-Si substrate, showing XRD spectra. **(c)** MgSe thin film on p-Si substrate AFM scans in 2D and (d) 3D with a scale of 2 × 2 μm, **(e)** MgSe thin film on p-Si substrate, FE-SEM image, and **(f)** EDX spectrum [25].

determined using the recorded XRD spectra along with the use of the commonly used Scherrer Equation shown below [26–29].

$$D = (0.9\lambda)/\beta \cos\theta \tag{1}$$

Table 1, [25] presents the calculated values for D and d crystallographic characteristics of MgSe thin film.

The knowledge obtained via AFM and SEM scans was employed to analyze the surface properties of the MgSe thin film on the p-Si. AFM is a valuable technique for analyzing the morphological characteristics of nanostructured thin films. The MgSe/p-Si structure is depicted in both two-dimensional and three-dimensional AFM micrographs in Fig. 2 (c) and (d), respectively, with scales of 2 × 2 μm. The two-dimensional (2D) image of the roughness profile of the MgSe thin film is shown in Fig. 2 (c). Grains of similar sizes can be noticed in these images and are evenly dispersed over the whole surface, as shown in Fig. 2 (c). The grains' sizes, shapes, and separations are uniform and spherical. It is possible to observe grains that resemble cylinders linked in Fig. 2(d); structures that this particular morphology could be employed in numerous optoelectronic. On the different side, the most crucial two factors for identifying a thin film surface morphology are known as the roughness, Ra, and the standard variation in the surface height within the specific area (root mean square, RMS) [30]. The surface roughness (RMS) values and Ra values have been derived from Fig. 2 (d) and are, correspondingly, 9.68 nm and 7.40 nm.

The FE-SEM micrograph and EDX spectra of the MgSe thin film on the p-Si substrate appear in Fig. 2 (e) and (f), respectively. MgSe thin film exhibits a consistent and homogenous surface shape, as can be observed in Fig. 2 (e). The thin film is made up of small, closely packed nanoparticles of a particular type. The grains displayed in the image are monodisperse spherical grains that resemble one another. The typical radius of spherical grains is around 20–50 nm. This outcome demonstrates the reasonable compatibility between the AFM and SEM findings. Furthermore, a high-quality nanocrystal formation of the MgSe thin film produced on the p-Si substrate is presented. The EDX chemical breakdown of the MgSe thin film that was produced on the p-Si substrate appears in Fig. 2 (f). It is obvious from the EDX measurements that bacteria synthesized MgSe nanoparticles.

Table 1
Evaluation of the structural characteristics of the MgSe thin film on the p-Si substrate [25].

(*hkl*)	FWHM	FWHM (rad)	Intensity (arb. u.)	2θ° (Observed)	d-values (nm)	Crystal size (D) nm	Crystal
(111)	0.1122	0.00196	1102.99	28.67	3,1102	73,03	Cubic
(200)	0.1496	0.00261	1642.88	32.59	2,7432	55,36	Cubic

3.2. Electrical properties of Ag/MgSe/p-Si/Al

3.2.1. I–V characteristics

The Ag/MgSe/p-Si/Al diode that we produced has been exposed to I–V evaluations in this section. We performed this by applying forward and reverse bias voltages at room temperature under both dark and illumination conditions. Using the data from these measurements, then the semi-logarithmic I–V curve was graphed and shown in Fig. 3. As analyzed from experimental measurements performed in darkness, the diode's characteristic I–V curve demonstrates that it exhibits good rectifying performance at values around +2 V from −2 V. The following describes the thermionic emission (T.E.) theory, which is a mathematical explanation of the theory that the forward bias current results thermally [31].:

$$I = I_o\left[exp\frac{q}{nkT}(V - IR_s)\right] \tag{2}$$

where T, V, k, n, I, R_s, and I_o are temperature (K), applied forward bias voltage, Boltzmann constant, the ideality factor, current-passing through the heterojunction, device's series resistance, the reverse saturation current, respectively. The reverse saturation current, I_o, however, is provided by the following expression,

$$I_o = A^*AT^2\ exp(-q\Phi_b / kT) \tag{3}$$

Herein, A and Φ_b are effective Richardson constant (32 A/cm^{2}K^2 for p-type Si), the diode's area, and the zero-bias barrier height, respectively [31–33]. Effective Richardson constant (32 A/cm^{2}K^2 for p-type Si), diode area, and zero-bias barrier height are each represented by the letters A^*, A and Φ_b, respectively [31–33]. The slope of the straight-line section of the semi-logarithmic I–V curve for forward bias may be used to calculate the ideality factor of a diode, which is indicated by n for pure thermionic emission. Moreover, its mathematical expression is given below:

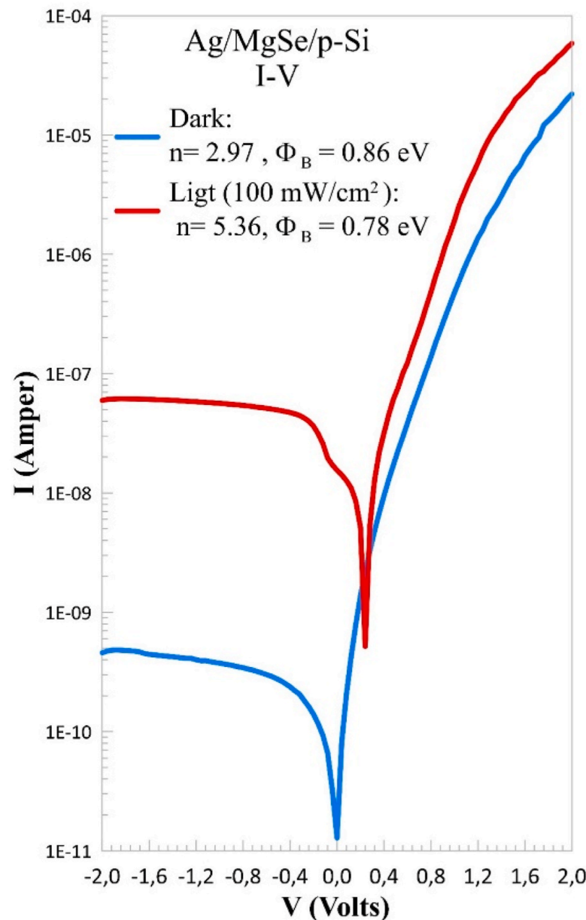

Fig. 3. Ag/MgSe/p-Si/Al device's current-voltage (I–V) characteristics under dark- and illumination (100 mW/cm^2).

$$n = \frac{q}{kT}\left[\frac{d(V - IR_s)}{dLn(I)}\right] \tag{4}$$

The values of n and Φ_b were determined to be (2.97–0,86 eV) and (5.36–0,78 eV), respectively, under dark and illumination circumstances.

In practice, it has been observed that the recognized value of n is more than unique. ($n > 1$). The reason for accepting the value of n in this way can be explained as follows: It is caused by the bias voltage decreasing across the interfacial layer that separates the metal from the semiconductor. As a result, it may be considered that the consequences of the bias voltage are what determine a diode's barrier height [30–32]. Furthermore, there are many reasons why the existence of bias-dependent barrier height or barrier inhomogeneity, interfacial recombination, or generation-recombination image forces lowering and metal-semiconductor interface impurities that divert the diode from the ideal n value [33–36]. Φ_b values (0,86 eV and 0.78 eV) found, as mentioned above, show that junction potential barrier height occurs in the interface (MgSe/p-Si interface) taking place between MgSe thin film layer and the p-Si semiconductor layer.

The influence of the interface states, which become active at high voltage values, causes the slopes of forward I–V graphics to rise significantly [37,38]. In this instance, the effect of series resistance is stated to depend on the states of the interface. As shown in Fig. 3, the interface states are particularly denser in measurements done under light, and the influence of R_s also rises appreciably. Therefore, in Fig. 4, the barrier height values may be controlled much more through interface states.

When the interfacial layer is sufficiently thick and the transmission probability between the interface states and the metal is low, it may be claimed that the effective barrier height, Φ_e, is voltage-dependent with respect to bias. This case reveals the appearance of interface states and between the interfacial layer and semiconductor interface is an interfacial insulator layer, and the formula for Φ_e is as follows [35].

$$\Phi_e = \Phi_b + \beta(V - IR_s) = \Phi_b + \left(1 - \frac{1}{n}\right)(V - IR_s) \tag{5}$$

here, β is the voltage coefficient of the barrier height that is actually employed, Φ_e, rather than the actual barrier height. As stated by Card and Rhoderick [35] in this circumstance, the ideality factor, n, rises above unity ($n > 1$) and its mathematical expression is provided,

$$n = 1 + \frac{\delta}{\varepsilon_i}\left[\frac{\varepsilon_s}{W_D} + qN_{ss}(V)\right] \tag{6}$$

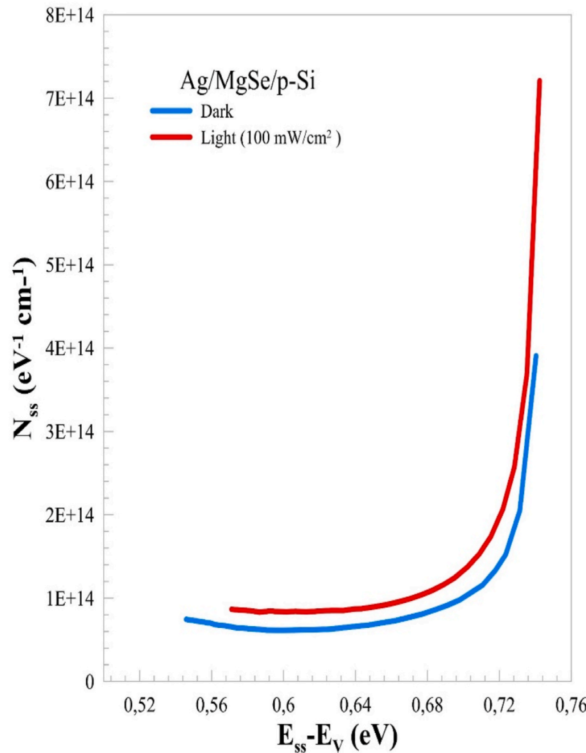

Fig. 4. Curves plotted energy distribution states, N_{ss}, of the Ag/MgSe/p-Si/Al diode versus (E_{ss}-E_V) at room temperature and dark-illumination (100 mW/cm^{-2}) conditions.

where is the thickness of the MgSe layer determined by the equation, and ε_i and ε_s are the dielectric constants of the semiconductor interfacial and layers, respectively.

($C_i = \varepsilon_i \varepsilon_S A / \delta$). W_D is the width of the space charge area, N_{SS} is the density of the interface states in equilibrium with the semiconductor, and C_i is the capacitance of the interfacial insulator layer for f = 1000 kHz in C–V measurements.

For p-type semiconductors, the equation for the energy of the interface states, or E_{SS}, in relation to the top of the valence band (E_V) at the semiconductor's surface is as follows:

$$E_{ss} - E_V = q(\Phi_e - V) \tag{7}$$

The energy distribution profile of the N_{SS} vs E_{SS}-E_V determined from the Ag/MgSe/p-Si structure's forward bias *I–V* characteristics in both dark and illumination circumstances is shown in Fig. 4. Obtaining this result, it was contemplated the bias dependency of the

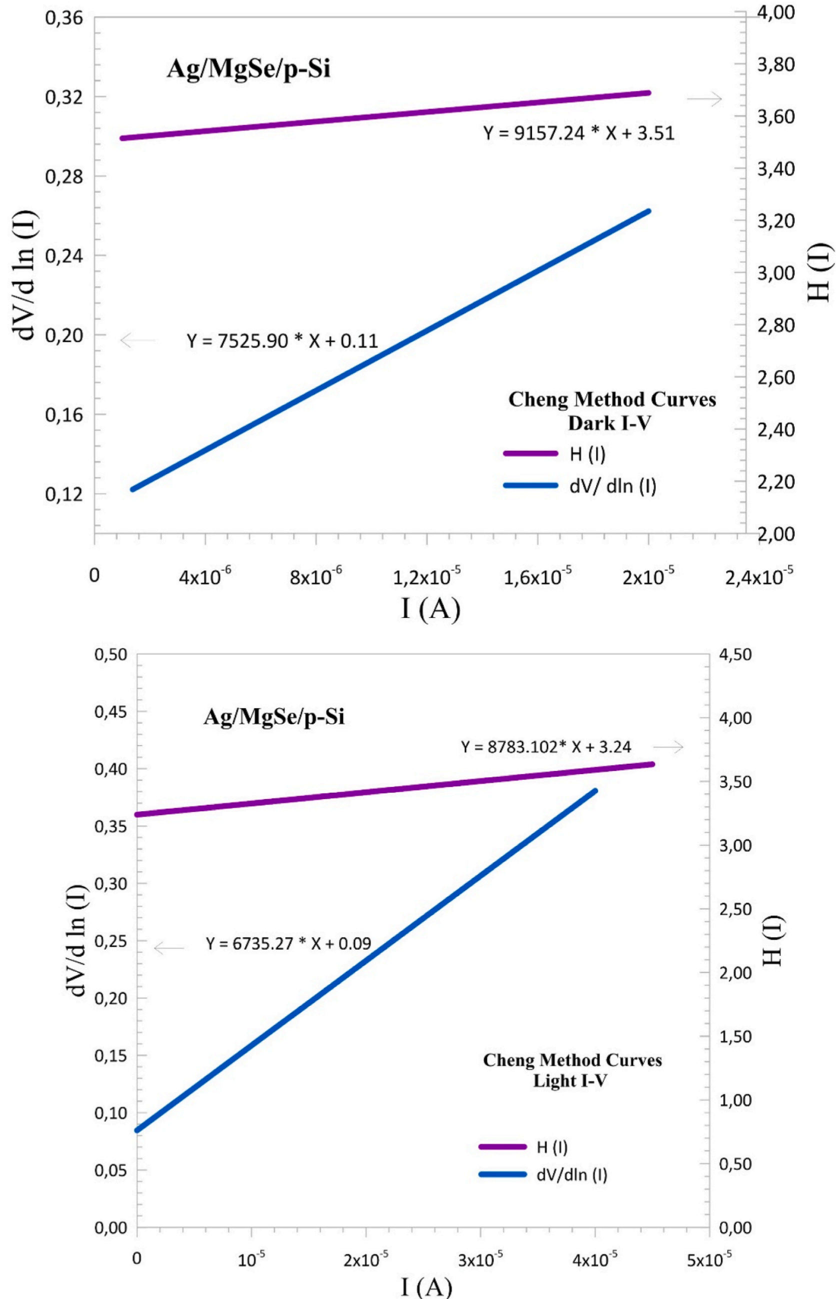

Fig. 5. Cheng Method characteristic of Ag/MgSe/p-Si/Al diode at room temperature (a) dark (b) illumination (100 mW/cm^{-2}).

effective barrier height (Φ_e) to the room temperature.

N_{SS} increases exponentially from the centre of the band gap energy levels to the top of the valence band, as seen in Fig. 4. Under both dark and light circumstances, the density distribution curves of the diode's interface states change from 0.54 eV to 0.73 eV and from 0.57 eV to 0.74 eV, respectively. For devices with 0.54-E_V to 0.73-E_V eV, the calculated values of the N_{ss} for dark and illumination circumstances are 7.80 × 1013 to 3.89 × 1014 eV^{-1} cm^{-2} and for devices with 0.57-E_V. to (0.74-E_V) eV, the calculated values are 8.76 × 10^{13} to 7.78 × 10^{14} eV^{-1} cm^{-2}, respectively. As expected, the number of interface states in the illuminated diode is larger than in the diode not illuminated.

The portions of these curves that correspond to low voltage become straight lines when the I–V curves are drawn on the semi-logarithmic paper using the data acquired from the applied forward bias voltage measurements. These straight lines significantly depart from linearity when the applied voltage is big enough due to the effects of R_s and N_{ss}. Cheung's functions [39] were employed to determine the values of series resistance, R_s, zero-bias barrier height, Φ_b, and ideality factor, n. Some aspects include,

$$\frac{dV}{d\,ln(I)} = IRs + n\left(\frac{kT}{q}\right) \tag{8}$$

$$H(I) = V - n\left(\frac{kT}{q}\right) ln\left(\frac{1}{AA^*T^2}\right) \tag{9}$$

$$H(I) = IR_s + n\Phi_b \tag{10}$$

Using information corresponding to the downward curvature portion of the forward bias I–V parameters, the barrier height, or Φ_b, is determined. The term "IR_S" refers to an equation that depicts a voltage dip throughout a diode's series resistances. The entire voltage dip across the series connection of the series resistances, Rs, in the diode is defined by the formula (V_d = V- IR_s).

Fig. 5 (a) and (b) exhibit dV/d(lnI) vs I and H(I) vs I curves produced using data from experimental observations carried out in dark and illuminated environments at room temperature, respectively. It is possible to determine the values of various parameters using the mathematical formula Eq. I0, which depicts a straight line corresponding to a downward curvature zone in the forward bias I–V features.

The slope and intercept of the straight line with the y-axis, respectively, are shown on the plot of dV/d(lnI) versus I, Rs, and nkT/q. Eq. 12's line relates to the plot of H (I) vs. I, and also its slope is equal to Φ_b (Fig. 5 (b). The slope of this curve could also be provided with the second determination of R_S., and it is possible to carry out this second value of the series resistance. by assessing Cheung's method's reliability.

For an Ag/MgSe/p-Si/Al diode at room temperature and under dark/illumination circumstances, the numerical values of certain parameters discovered from experimental I–V measurements and utilizing the Cheung Method are provided in Table 2.

Herein, using the slopes of the straight lines and the y-axis intersection of the dV/dlnI versus I graphs for dark-illumination conditions, R_s and n values were found (7525.90–6535.27) Ω and (4.24–3.50), respectively. Also, using the n values of (4.24–3.50), the slope and y-axis intersection of graphs of the values for the barrier height, Rs, and H(I) vs. I could be found as (0.83–0.92) eV and (9157.54–8783.10) Ω, respectively. Furthermore, Eqs. (10) and (12) are used to derive the values of series resistances. As can be observed, the value of Rs acquired from H(I)–I plots and the value received from dV/d(lnI)-I plot is in a fair amount of agreement. This outcome attests to the applicability of Cheung's approach [40–43].

3.2.2. Ag/MgSe/p-Si/Al diode capacity-voltage properties

In order to figure out the values of some parameters corresponding to the C–V characteristics of the diode, we performed C–V measurements using forward and reverse bias voltages varying in the range from −4 to +4 V with 0,02 V stages at room temperature and in the dark, in addition to using various application frequencies (50 kHz, 100 kHz, 200 kHz, 500 kHz ve 1000 kHz). The Ag/MgSe/p-Si/Al structure's C–V and C^2–V curves are depicted in Figs. 6 and 7, respectively, utilizing experimental forward and reverse bias C–V measurements.

The capacitance of a diode corresponding to the region named depletion region between the metal-semiconductor junctions is given [27]:

Table 2
The Ag/MgSe/p-Si/Al device's I–V and Cheung Method parameters were employed to compute the numerical measurements for various parameters under ambient temperature and dark-illumination conditions.

Dark						Illumination (100 W/cm^{-2})					
I–V curve		$\frac{dV}{d\ln(I)}$		H (I)		I–V curve		$\frac{dV}{d\ln(I)}$		H (I)	
n	Φ_b (eV)	n	R_S (Ω)	Φ_b (eV)	R_S	n	Φ_b (eV)	n	R_S (Ω)	Φ_b (eV)	Rs (Ω)
2.97	0.86	4.24	7525.90	0.83	9157.24	5.36	0.78	3.50	6735.27	0.92	8783.10

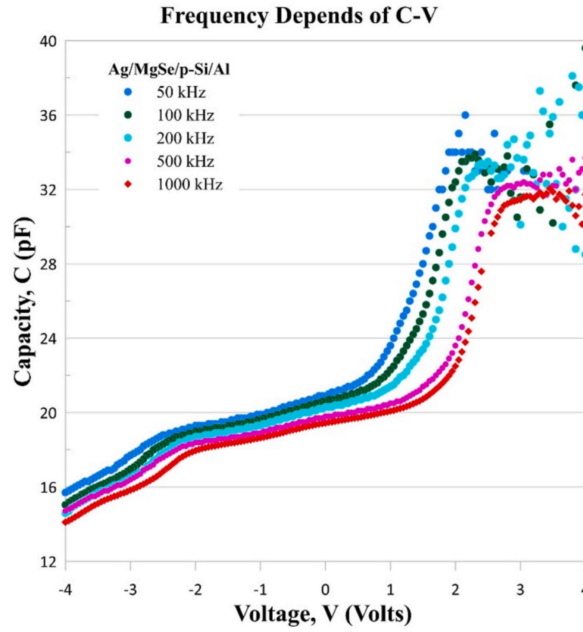

Fig. 6. C–V characteristics of an Ag/MgSe/p-Si/Al device with forward and reverse bias at ambient temperature.

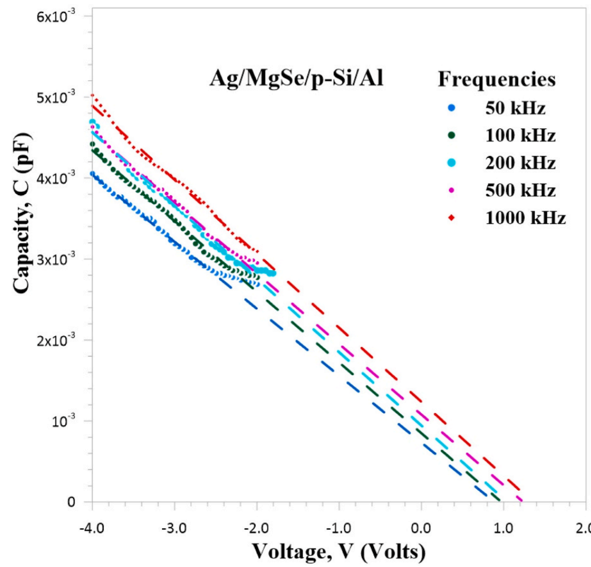

Fig. 7. As a frequency-dependent variable, the reverse bias of C^{-2}–V characteristics of Ag/MgSe/p- Si/Al diode.

$$C = \left[\frac{q\varepsilon_s N_a A^2}{2\left(V_d - V - \frac{kT}{q}\right)} \right]^{1/2} \tag{11}$$

where V_d, V, A, N_α, and ε_s, are the zero feeding diffusion potential, applied voltage, the effective area of the diode, the concentration of the ionized acceptor atoms, and the dielectric constant of the semiconductor (p-Si), respectively.

The equation, which will be employed to calculate the value of N_α, is derived from Eq. (13),

$$N_a = \frac{2}{q\varepsilon_S \varepsilon_o A^2} \left[\frac{d}{dV} \left(\frac{1}{C^2} \right) \right]^{-1} \tag{12}$$

The numerical value of the concentration of acceptor atoms, N_α, is calculated using Eq. (14). Besides, Fermi energy levels and potential barrier heights can be found by using the equations derived based on the strengths of $C^{-2-}V$ curves in Fig. 7, and they are given below, respectively,

$$E_F = \frac{kT}{q} ln\left(\frac{N_a}{N_V}\right) \tag{13}$$

$$\Phi_b = V_d + \frac{kT}{q} ln\left(\frac{N_a}{N_V}\right) \tag{14}$$

but, to find the numerical values of the parameters mentioned above, it is necessary to know the value of the concentration of valence band atoms, $N_{V.}$ The numerical value of N_V. (for room temperature $8.10^{\ 14}$ cm^{-3}) is found from the well-known expression,

$$N_V = 2\left[\frac{(2m_h * kT)^{3/2}}{\hbar^3}\right] \tag{15}$$

The C–V curves plotted using the data from these measurements are displayed in Fig. 6. According to this graph, diode capacitance is strongly frequency dependent, and also it is seen that there are inversion depletion and agglomeration regions on each of the curves. For various frequency levels, these modifications may be seen on the C–V curves relating to the depletion and agglomeration zones. The localized interface states, N_{SS}, in the forbidden energy gap between the MgSe thin film and Si crystal layers, may be responsible for the splittings seen in the depletion area on C–V curves [44].

C–V values vary on applied voltages as well as frequency, as can be shown in Fig. 6, C–V curves reach seen pick points in a small applied potential region (2.2–3.2 V). Furthermore, it is seen that these pick points decrease with increasing frequency, and in this case, the curves reach the pick points at the higher voltage values. Therefore, the position of the pick shifts towards high voltages resulting from the restructuring and rearrangement of surface states. The existence of interface states in the agglomeration and series resistance, as well as the decline in C values observed in Fig. 6, which depicts the samples' inductive behaviour after picking, are the additional elements, however, that are responsible for this change [45–48].

High C–V values at low frequencies are also due to the interface states [48]. The N_{SS} ac signal is easily tracked, achieving excessive capacitance and conductivity levels in accordance with the reported values if the C–V measurements are carried out adequately at low frequencies [49]. The effect of adding the interface states to the measured capacitance of the capacitor, on the other hand, is very minor and may be ignored in this instance since N_{SS} cannot follow an ac signal [48].

The C^{-2}-V curves for various frequencies were used to compute numerical values for some of the electrical characteristics of the manufactured diode previously mentioned. Table 3 indicates that these parameters depend rather strongly on the frequency, as is also observed previously [50]. The other significant result from Table 3 is that the numerical values of N_a of Ag/MgSe/p-Si/Al diode decrease as frequency rises. This decline is brought on by charges that are concentrated in the interface layer and are unable to follow the high frequency due to the frequency-dependent increase in Φ_b. Together with all of these findings, the value of E_F is constant. The image charge effect can interpret in this case due to Fermi level pinning staying on its position without changing [51].

4. Conclusion

In our earlier study publication, we described the first time that MgSe compound NPs were produced using the bacterial (*P. aeruginosa* OG1) green synthesis approach. Thereafter, nanocrystalline MgSe thin films on p-Si and glass substrates are studied. To explore effects under illumination, interfacial thin films in an Au/MgSe/p-Si/Al device structure were fabricated in the latter. Originally, XRD, AFM, UV–Vis Spectrophotometer, and FE-SEM with EDS methods were used to explore the characteristics of nanocrystalline thin films. Our findings demonstrated that the MgSe nanocrystalline thin films were uniformly polycrystalline with nanoscale grain size. After that, to produce a layered Ag/MgSe/p-Si/Al device, a thin MgSe film was placed between the metal (Ag) and p-type Si. I–V measurements were then taken at room temperature when the device (diode) was in the dark and illuminated (100 mW/cm^{-2}) for evaluation. In dark and illuminated circumstances, the numerical values of two important diode parameters, such as n and Φ_b, were revealed to be (2.97–0,86) eV and (5.36–0,78) eV, respectively. Under illumination, the ideality factor, n, was observed to grow significantly more than it did in the dark. It is noted that, under the illumination situation, the value of barrier height drops. This outcome is a result of rising interface state density levels. Furthermore, it was proved that the interface state density value obtained under illumination is larger than the one obtained under dark, and they are (7.78×10^{14} eV^{-1} cm^{-2}) and (8.76×10^{13} eV^{-1} cm^{-2}), respectively. Moreover, values for series resistance, barrier height, and ideality factor were determined using Cheung's technique to contrast the two approaches. In experiments, the diode's series resistances for both illumination and dark conditions were determined. The goal is to demonstrate that growth in the thickness of the interface layer and the density of the interface state may be responsible for the rise in the series resistance value. C–V measurements of the diode were conducted by applying different voltages varying from −4 V to +4V and frequencies (50-100-200-500-1000 kHz). Subsequently, using the data from the measurements, C^{-2}-V visuals, including linear curves, were produced. The values of basic electronic structure and some parameters (N_α, E_F (eV), V (eV)d and Φ_b (eV)) were obtained for applied frequency in the inversion region using the intercept sites for linear segments of linear parts and slopes of C^{-2}-V graphics. High capacity values obtained at low frequencies can be attributed to existing interface states and their lifetimes. These findings demonstrate that MgSe nanocrystalline films were produced with the bacterial-produced method. Ag/MgSe/p-Si/Al device structure has been developed and shown a remarkable photoresponse and steady rectifying property. Green synthesis

Table 3
Several parameters were calculated from the Ag/MgSe/p-Si/Al diode's C–V properties at room temperature.

Frequencies (kHz)	Nα (10^{14} cm^{-3})	E_F (eV)	V_d (eV)	Φ_b (eV)
50	2.35	0.032	0.89	0.92
100	2.22	0.033	0.97	1.004
200	2.14	0.034	0.99	1.02
500	2.38	0.031	1.23	1.26
1000	2.12	0.034	1.35	1.38

methods for the production of these nanocrystalline materials have the potential to offer low-cost alternatives for photosensitive applications. Therefore, they can be used as photodiodes, photosensors and quantum-good laser diodes in industrial applications.

Funding

Princess Nourah Bint Abdulrahman University Researchers Supporting Project number (PNURSP2023R111), Princess Nourah Bint Abdulrahman University, Riyadh, Saudi Arabia. The work of the author AE and APC was covered by "Dungareede Jos" University of Galati, Romania.\

Data availability statement

Data will be made available on request.

CRediT authorship contribution statement

T. Çakıcı: Conceptualization, Investigation, Writing – original draft. **Ö. Gür Özdal:** Conceptualization, Software, Writing – original draft. **N. Almousa:** Funding acquisition, Methodology, Project administration, Writing – review & editing. **F. Yıldız:** Data curation, Resources, Software, Writing – original draft. **E. Kavaz Perişanoğlu:** Methodology, Validation, Visualization, Writing – original draft. **H. Khalil:** Investigation, Validation, Writing – review & editing. **Antoaneta Ene:** Formal analysis, Funding acquisition, Investigation, Writing – review & editing. **Hesham M.H. Zakaly:** Methodology, Software, Supervision, Writing – review & editing.

Declaration of competing interest

The authors declare that they have no known competing financial interests or personal relationships that could have appeared to influence the work reported in this paper.

Acknowledgements

The authors express their gratitude to Princess Norah bint Abdulrahman University Researchers Supporting Project number (PNURSP2023R111), Princess Nourah bint Abdulrahman University, Riyadh, Saudi Arabia.

References

[1] G. Chen, I. Roy, C. Yang, P.N. Prasad, Nanochemistry and nanomedicine for nanoparticle-based diagnostics and therapy, Chem. Rev. 116 (2016) 2826–2885, https://doi.org/10.1021/acs.chemrev.5b00148.
[2] M.R. Bindhu, M. Umadevi, M.K. Micheal, M.V. Arasu, N.A. Al-Dhabi, Structural, morphological and optical properties of MgO nanoparticles for antibacterial applications, Mater. Lett. 166 (2016) 19–22, https://doi.org/10.1016/j.matlet.2015.12.020.
[3] A. K Mittal, J. Bhaumik, S. Kumar, U.C. Banerjee, Biosynthesis of silver nanoparticles: elucidation of prospective mechanism and therapeutic potential, J. Colloid Interface Sci. 415 (2014) 39–47, https://doi.org/10.1016/j.jcis.2013.10.018.
[4] J. Singh, T. Dutta, K.H. Kim, M. Rawat, P. Samddar, P. Kumar, 'Green' synthesis of metals and their oxide nanoparticles: applications for environmental remediation, J. Nanobiotechnol. 16 (2018) 84, https://doi.org/10.1186/s12951-018-0408-4.
[5] P. Singh, Y.J. Kim, D. Zhang, D.C. Yang, Biological synthesis of nanoparticles from plants and microorganisms, Trends Biotechnol. 34 (2016) 588–599, https://doi.org/10.1016/j.tibtech.2016.02.006.
[6] G. Gahlawat, A.R. Choudhury, A review on the biosynthesis of metal and metal salt nanoparticles by microbes, RSC Adv. 9 (2019) 12944–12967, https://doi.org/10.1039/C8RA10483B.
[7] M. Ozdal, O.G. Ozdal, O.F. Algur, Isolation and characterization of α-endosulfan degrading bacteria from the microflora of cockroaches, Pol. J. Microbiol. 65 (2016) 63–68, https://doi.org/10.5604/17331331.1197325.
[8] T. Çakıcı, M. Ozdal, M. Kundakcı, R. Kayalı, ZnSe and CuSe NP's by microbial green synthesis method and comparison of IV characteristics of Au/ZnSe/p-Si/Al and Au/CuSe/p-Si/Al structures, Mater. Sci. Semicond. Process. 103 (2019), 104610, https://doi.org/10.1016/j.mssp.2019.104610.
[9] M. Kitching, M. Ramani, E. Marsili, Fungal biosynthesis of gold nanoparticles: mechanism and scale up, Microb. Biotechnol. 8 (2015) 904–917, https://doi.org/10.1111/1751-7915.12151.
[10] S.A. Kumar, M.K. Abyaneh, S.W. Gosavi, S.K. Kulkarni, R. Pasricha, A. Ahmad, M.I. Khan, Nitrate reductase-mediated synthesis of silver nanoparticles from $AgNO_3$, Biotechnol. Lett. 29 (2007) 439–445, https://doi.org/10.1007/s10529-006-9256-7.
[11] Z. Vaseghi, A. Nematollahzadeh, O. Tavakoli, Green methods for the synthesis of metal nanoparticles using biogenic reducing agents: a review, Rev. Chem. Eng. 34 (2018) 529–559.
[12] J. Liu, H. Zhan, N. Wang, et al., Palladium nanoparticles on covalent organic framework supports as catalysts for suzuki–miyaura cross-coupling reactions, ACS Appl. Nano Mater. (2021).

[13] H. Morkoc, S. Strite, G.B. Gao, M.E. Lin, B. Sverdlow, M. Burns, Large-band-gap SiC, III-V nitride, and II-VI ZnSe-based semiconductor device technologies, J. Appl. Phys. 76 (1994) 1363, https://doi.org/10.1063/1.358463.

[14] R.F.C. Farrow, G.R. Jones, G.H. Williams, I.M. Young, Molecular beam epitaxial growth of high structural perfection, heteroepitaxial CdTe films on InSb (001), Appl. Phys. Lett. 39 (1981) 954, https://doi.org/10.1063/1.92616.

[15] A. U Uable, A. N Bargal, Characterization of nanostructured photosensitive (NiS)x(CdS)(1−x) composite thin films grown by successive ionic layer adsorption and reaction (SILAR) route, Mater. Res. Bull. 46 (2011) 1000–1010, https://doi.org/10.1016/j.materresbull.2011.03.016.

[16] U. Ubale, Effect of complexing agent on growth process and properties of nanostructured Bi2S3 thin films deposited by chemical bath deposition method, Mater. Chem. Phys. 121 (2010) 555–560, https://doi.org/10.1016/j.matchemphys.2010.02.021.

[17] M.W. Wang, M.C. Phillips, J.F. Swenberg, E.T. Yu, J.O. McCaldin, T.C. McGill, n-CdSe/p-ZnTe based wide band-gap light emitters: numerical simulation and design, J. Appl. Phys. 73 (1993) 4660–4668, https://doi.org/10.1063/1.352761.

[18] A. Shen, G. Chen, K. Zhao, J.T. Lai, M.C. Tamargo, Metastable CdSe/MgSe quantum wells prepared by MBE with near I.R. intersubband absorption, J. Vac. Sci. Technol. B 31 (2013), 03C103, https://doi.org/10.1116/1.4789478.

[19] G. Chen, M.C. Tamargo, A. Shen, Optimisation of barrier layer thickness in MgSe/CdSe quantum wells for intersubband devices in the near infrared region, J. Appl. Phys. 118 (2015), 165707, https://doi.org/10.1063/1.4934858.

[20] J. De Jesus, G. Chen, L.C. Hernandez-Mainet, A. Shen, M.C. Tamargo, Strain compensated CdSe/ZnSe/ZnCdMgSe quantum wells as building blocks for near to mid-IR intersubband devices, J. Cryst. Growth 425 (2015) 207–211, https://doi.org/10.1016/j.jcrysgro.2014.12.021.

[21] T. Çakıcı, Ö. Özdal, Synthesizing of MgSe complex nanoparticle via bacteria and characterisation of fabricated MgSe/p-Si structure, Acta Phys. Pol., A 140 (1) (2021).

[22] A.U. Ubale, Y.S. Sakhare, Thickness dependent physical properties of chemically deposited nanocrystalline MgSe thin films deposited at room temperature by solution growth method, Mater. Sci. Semicond. Process. 16 (2013) 1769–1774, https://doi.org/10.1016/j.mssp.2013.06.015.

[23] A.U. Ubale, Y.S. Sakhare, Growth of nanocrystalline MgSe thin films by spray pyrolysis, Vacuum 99 (2014) 124–126, https://doi.org/10.1016/j.vacuum.2013.05.004.

[24] Y.S. Sakhare, N.R. Thakare, A.U. Ubale, Influence of quantity of spray solution on the physical properties of spray deposited nanocrystalline MgSe thin films, St Petersburg Polytech Univ J: Phys Math. 2 (2016) 17–26.

[25] T. Çakıcı, B. Güzeldir, M. Sağlam, Temperature dependent of electrical characteristics of Au/n-GaAs/In Schottky diode with In_2S_3 interfacial layer obtained by using spray pyrolysis method, J. Alloys Compd. 646 (2015) 954–965, https://doi.org/10.1016/j.jallcom.2015.06.017.

[26] D. Raoufi, A. Kiasatpour, H.R. Fallah, A.S.H. Rozatian, Surface characterization and microstructure of ITO thin films at different annealing temperatures, Appl. Surf. Sci. 253 (2007) 9085–9090, https://doi.org/10.1016/j.apsusc.2007.05.032.

[27] E.H. Rhoderick, R.H. Williams, Metal–Semiconductor Contacts, Oxford University Press, New York, 1988.

[28] T. Çakıcı, Investigation of Go: Cu nanoparticles produced by green systemization method and fabrication of Au/Go: Cu/p-Si/al diode, J. Mol. Struct. 1199 (2020), 126945, https://doi.org/10.1016/j.molstruc.2019.126945.

[29] T. Çakıcı, Production and characterization of G.O.: Se nanoparticles produced by biosynthesis method and current-voltage characteristics of the Ag/G.O.: Se/p-Si device developed by using G.O.: Se nanoparticles, European J. Sci. Technol. 17 (2019) 1367–1374, https://doi.org/10.31590/ejosat.665070.

[30] T. Çakıcı, M. Sağlam, The effects of growth parameters on electrical characteristics of In_2S_3/n-InP junctions with In_2S_3 interfacial layer obtained by chemical spray pyrolysis method, Mater. Today: Proc. 3 (2016) 1262–1270, https://doi.org/10.1016/j.matpr.2016.03.069.

[31] A. Türüt, N. Yalçın, M. Sağlam, Parameter extraction from non-ideal C− V characteristics of a Schottky diode with and without interfacial layer, Solid State Electron. 35 (1992) 835–841, https://doi.org/10.1016/0038-1101(92)90286-L.

[32] T. Çakıcı M. Sağlam, B. Güzeldir, The comparison of electrical characteristics of Au/n-InP/In and Au/In_2S_3/n-InP/In junctions at room temperature, Mater, Sci. Engineer. B 193 (2015) 61–69, https://doi.org/10.1016/j.mseb.2014.11.003.

[33] İ. Dökme, Ş. Altındal, On the intersecting behaviour of experimental forward bias current-voltage (I–V) characteristics of Al/SiO_2/p-Si (MIS) Schottky diodes at low temperatures, Semicond. Sci. Technol. 21 (2006) 1053, https://doi.org/10.1088/0268-1242/21/8/012.

[34] İ. Dökme, The effect of series resistance and oxide layer formed by thermal oxidation on some electrical parameters of Al/SiO_2/p-Si Schottky diodes, Phys. B Condens. Matter 388 (2007) 10–15, https://doi.org/10.1016/j.physb.2006.04.032.

[35] H.C. Card, E.H. Rhoderick, Studies of tunnel MOS diodes I. Interface effects in silicon Schottky diodes, J. Phys. D Appl. Phys. 4 (1971) 1589.

[36] A. Singh, K.C. Reinhardt, W.A. Anderson, Temperature dependence of the electrical characteristics of Yb/p-InP tunnel metal-insulator-semiconductor junctions, J. Appl. Phys. 68 (1990) 3475–3483, https://doi.org/10.1063/1.346358.

[37] M.E. Aydın, T. Kılıçoğlu, A. Akkılıç, H. Hoşgören, The calculation of electronic parameters of an Au/β-carotene/n-Si Schottky barrier diode, Phys. B Condens. Matter 381 (2006) 113–117, https://doi.org/10.1016/j.physb.2005.12.254.

[38] M.A. Ebeoğlu, T. Kılıçoğlu, M.E. Aydın, Low-and high-frequency C–V characteristics of the contacts formed by adding a solution of the nonpolymeric organic compound on p-type Si substrate, Phys. B Condens. Matter 395 (2007) 93–97, https://doi.org/10.1016/j.physb.2007.02.063.

[39] S.K. Cheung, N.W. Cheung, Extraction of Schottky diode parameters from forward current-voltage characteristics, Appl. Phys. Lett. 49 (1986) 85–87, https://doi.org/10.1063/1.97359.

[40] B. Akkal, Z. Benemara, A. Boudissa, N.B. Bouiadjra, M. Amrani, L. Bideux, B. Gruzza, Modelization and characterization of Au/InSb/InP Schottky systems as a function of temperature, Mater. Sci. Eng., B 55 (1998) 162–168, https://doi.org/10.1016/S0921-5107(98)00168-8.

[41] M.Y. Feteha, M. Soliman, N.G. Gomaa, M. Ashry, Metal-insulator-semiconductor solar cell under gamma irradiation, Renew. Energy 26 (2002) 113–120, https://doi.org/10.1016/S0960-1481(01)00102-1.

[42] L. Beji, J.T. Ben, Z. Harrabi, A. Laribi, A. Missaoui, A. Bouazizi, DC A.C, Electrical characteristics of porous GaAs/p^+–GaAs heterostructure, Vacuum 80 (2006) 480–487, https://doi.org/10.1016/j.vacuum.2005.08.024.

[43] A. Tataroğlu, Ş. Altındal, Analysis of interface states and series resistance of MIS Schottky diodes using the current–voltage (I–V) characteristics, Microelectron. Eng. 85 (2008) 233–237, https://doi.org/10.1016/j.mee.2007.05.043.

[44] H. Tecimer, S.O. Tan, Ş. Altındal, Frequency-dependent admittance analysis of the metal–semiconductor structure with an interlayer of Zn-doped organic polymer nanocomposites, IEEE Trans. Electron. Dev. 65 (2017) 231–236, https://doi.org/10.1109/TED.2017.2778023.

[45] S.M. Sze, Physics of Semiconductor Devices, second ed., John Wiley, New York, 1981, p. 294.

[46] S.A. Yerişkin, H.İ. Ünal, B. Sarı, Electrical and dielectric characteristics of Al/polyindole Schottky barrier diodes. II. Frequency dependence, J. Appl. Polym. Sci. 120 (2011) 390–396, https://doi.org/10.1002/app.33148.

[47] S. Demirezen, A. Kaya, Ş. Altındal, İ. Uslu, The energy density distribution profile of interface traps and their relaxation times and capture cross sections of Au/GO-doped PrBaCoO nanoceramic/n-Si capacitors at room temperature, Polym. Bull. 74 (2017) 3765–3781, https://doi.org/10.1007/s00289-017-1925-2.

[48] E.H. Nicollian, J.R. Brews, Metal Oxide Semiconductor (MOS) Physics and Technology, 3nd, Wiley, New York, 1982, pp. 225–237.

[49] B. Kinaci, S. Özçelik, B. Kınacı, S. Özçelik, Temperature dependent capacitance-voltage and conductance-voltage characteristics of Au/TiO2 (rutile)/n-Si MIS structure at 1 Mhz, J. Electron. Mater. 42 (2013) 1108–1113, https://doi.org/10.1007/s11664-013-2524-0.

[50] M. Sharma, S.K. Tripathi, Frequency and voltage dependence of admittance characteristics of Al/Al_2O_3/PVA: n-ZnSe Schottky barrier diodes, Mater. Sci. Semicond. Process. 41 (2016) 155–161, https://doi.org/10.1016/j.mssp.2015.07.028.

[51] R.T. Tung, Comment on "Numerical study of electrical transport in homogeneous Schottky diodes, J. Appl. Phys. 88 (2000) 7366–7367, https://doi.org/10.1063/1.369185.